Interactions between gas slug ascent and exchange flow in the conduit of persistently active volcanoes

Zhipeng Qin [1], Frances M Beckett[2], Alison C Rust[3], Jenny Suckale [4,5,6]

[1]School of Mechanical Engineering, Guangxi University, Nanning, Guangxi, 53004, PR China

[2]Met Office, Exeter, EX1 3PB, UK

[3]School of Earth Sciences, University of Bristol, Bristol, UK

[4]Department of Geophysics, Stanford University, Stanford, California 94305, USA

[5]Department of Civil and Environmental Engineering, Stanford University, Stanford, California 94305, USA

[6]Institute for Computational and Mathematical Engineering, Stanford University, Stanford, California 94305, USA

Key Points:

- Experiments and simulations demonstrate the value of coupling slug ascent and exchange flow in models of persistently active volcanoes.
- A single slug can pass through an exchange flow without creating a lasting disruption because it ascends much faster than the core magma.
- Sequential slug ascent disrupts the mass balance of the exchange flow, potentially contributing to transitions in eruptive regimes.

Corresponding author: Zhipeng Qin, zhipengq@gxu.edu.cn

This article has been accepted for publication and undergone full peer review but has not been through the copyediting, typesetting, pagination and proofreading process, which may lead to differences between this version and the Version of Record. Please cite this article as doi: 10.1029/2021JB022120.

Abstract

Many volcanoes around the world are persistently active with continuous degassing for years or even centuries, sometimes exceeding historic records. Such long-term stability contrasts with short-term instability, reflected in eruptive episodes that punctuate passive degassing. These two aspects of persistent activity, long-term stability as opposed to short-term instability, are often conceptualized through two distinct model frameworks: Exchange-flow in volcanic conduits is commonly invoked to explain the long-term thermal balance and sustained passive degassing, while the ascent of large gas slugs is called upon to understand explosive eruptions. While typically considered separately, we propose here that both flow processes could occur jointly in the conduits of persistently active volcanoes and in transient connections between subvolcanic melt lenses. To understand the dynamic interplay between exchange flow and slug ascent, we link analogue laboratory experiments with direct numerical simulations. We find that the two flows superimpose without creating major disruptions when only considering the ascent of a single gas slug. However, the sequential ascent of multiple gas slugs is disruptive to the ambient exchange flow, because it may entail continual buildup of buoyant magma at depth. While our study focuses on the laboratory scale, we propose that the dependence of exchange-flow stability on sequential slug ascent is relevant for understanding why explosive sequences are sometimes followed by effusive eruptions. Taken together, our work suggests that integrating exchange flow and slug ascent could provide a more complete understanding of persistently active volcanoes than either model framework offers in isolation.

Plain Language Summary

Many volcanoes around the world erupt frequently, some of them on a daily basis, emitting large quantities of gas, but erupting relatively little magma. Gas fluxes remain high even when there is no eruptive activity, suggesting that magma acts as a conveyer belt that transports gas bubbles to the surface and returns to depth degassed, having lost its buoyant cargo. The framework quantifying this process is called the exchange-flow model. It explains observations of high heat and gas flux, but raises a new question: If gas transport is efficient enough to allow continuous gas emission without eruptive activity, why does not all of the gas escape in this way? One possibility is that gas accumulates into large bubbles that exceed the capacity of the magmatic conveyer belt and

rise to the surface by themselves, expanding and accelerating on the way. The framework quantifying this process is called the slug model. Here, we integrate these two models by studying their interactions in laboratory experiments and computer simulations. We find that one can impede the functionality of the other, which could be relevant for transitions in eruptive regimes, such as a switch from episodic explosions to outpourings of magma.

1 Introduction

Many volcanoes around the world erupt frequently, sometimes as frequently as every few minutes (Ripepe et al., 2002; Harris & Ripepe, 2007; Palma et al., 2008; C. Oppenheimer et al., 2011). Periods of unrest tend to alternate with extended periods of relative quiescence (Shinohara, 2008), creating a wide spectrum of behavior from continuous passive degassing to intermittent explosive or effusive eruptions and more rare, paroxysmal eruptions that emerge with little or no clear precursory activity (e.g., Albert et al., 2016; Passarelli & Brodsky, 2012). The transitions between different eruptive regimes are sudden and unpredictable, creating significant uncertainty in risk assessments (e.g., Ripepe et al., 2017). A central challenge in understanding the activity at persistently active volcanoes is hence to explain the great variety in eruptive styles and the processes that govern the transition between them.

Frequent or persistent activity is often closely related to excessive degassing (Shinohara, 2008), which means that the volcanoes emit larger quantities of gas than can be dissolved in the volume of magma erupted during the various eruptive regimes. Example volcanoes exhibiting this kind of behavior include, but are not limited to, Stromboli (Italy), Masaya (Nicaragua), Villarrica (Chile), Izu Oshima (Japan), Erebus (Antarctica), and Yazur (Vanuatu) (Allard et al., 1994; Palma et al., 2008; Kazahaya et al., 1994; C. Oppenheimer et al., 2011; Stoiber & Williams, 1986; Firth et al., 2014). Given that these volcanoes degas much more magma than they erupt, the majority of degassed magma must be transported back down to depth after degassing. Passive degassing occurs continuously, so the ascent of volatile-rich and the descent of volatile-poor magma must occur simultaneously in the volcanic conduit, leading to what is commonly referred to as exchange flow.

In exchange flow, the upward flux of volatile-rich magma approximately equals the downward flux of degassed magma, which can create a balanced, relatively steady flow field (Stevenson & Blake, 1998). It provides both the relatively large surface gas flux suggested by observations and the heat flux necessary to explain how persistently active volcanoes remain intermittently active over centuries or even millennia (Francis et al., 1993; Kazahaya et al., 1994). However, exchange flow does not offer an obvious explanation for why persistently active volcanoes erupt in the first place, rather than emitting all of the gas passively. It is hence not surprising that the eruptive behavior at persistently active volcanoes is typically explained through an entirely different conceptual framework, commonly referred to as the slug model.

The slug model is based on the insight that exsolved volatiles separate from the magmatic phase, forming a gas phase with its own dynamics (Vergniolle & Jaupart, 1986). The existence of a separate gas phase creates different dynamic regimes, from bubbly flow to slug flow and churn flow, that could be associated with different eruptive regimes, as first suggested by Jaupart and Vergniolle (1988). However, other factors such as gas overpressure (James et al., 2004, 2008; Del Bello et al., 2012; Allard, 2010) and crystallization in the upper portion of the conduit (Del Bello et al., 2015; Suckale et al., 2016; J. Oppenheimer et al., 2020) may contribute as well. While the presence of a separate gas phase is undoubtedly important for eruptions dynamics, it is not entirely clear how the transition between different eruptive regimes, and the variability of behavior within a given eruptive regime, is related to flow processes in the volcanic conduit.

Since persistently active volcanoes are characterized by both large heat and gas flux on the multi-decadal or century scale and by sometimes violent eruptive activity on the minute or hourly scale, it would be desirable to develop a unified model framework able to capture both limits. The two models integrate naturally in the limit of long temporal scales: In exchange flow, the buoyancy of the ascending magma is due to the presence of small gas bubbles that decouple and degas upon reaching the free surface, leaving behind degassed, dense magma that sinks back down to depth (Francis et al., 1993; Kazahaya et al., 1994; Stevenson & Blake, 1998). The slug model also associates passive degassing with the steady ascent of small bubbles (e.g., Jaupart & Vergniolle, 1988, 1989; Vergniolle & Mangan, 2000). In the limit of short temporal scales, the integration of the two frameworks is less obvious: A rapidly ascending gas slug could perturb the

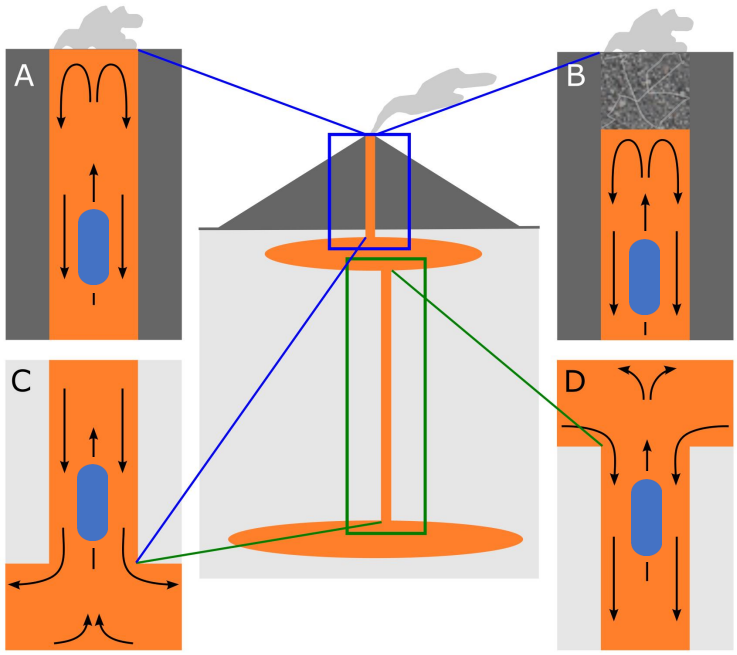

Figure 1. Conceptual sketch of where exchange flow and slug ascent could occur within and below the volcanic edifice. Possible exchange-flow domains include both the uppermost portion of the volcanic plumbing system (blue box) and intermediate depths where vertical connections might transiently connect multiple melt lenses (green box). Ascending slugs are shown in light blue. A: At open-vent volcanoes or lava lakes such as at Kīlauea, Hawaii, backflow can sometimes be observed directly (Stovall et al., 2009). B: At some persistently active volcanoes such as Stromboli volcano, Italy, the upper conduit is partially crystallized and exchange flow likely occurs underneath, removed from direct observation. C: Base of the model domain where exchange flow connects to a storage reservoir or melt lens. D: Top of the model domain when exchange flow at intermediate depth connects two melt lenses.

.

precarious balance of the exchange flow interface (Hickox, 1971), potentially triggering flow switching (Suckale et al., 2018).

The goal of this paper is to understand the dynamic interplay between slug ascent in exchange flow by linking analogue laboratory experiments and direct numerical simulations. Our study is motivated by the possibility that the integration of slug ascent and exchange flow into a single model framework may provide the basis for a more complete understanding of persistently active volcanoes than either of the two models in iso-

lation. We hypothesize that the presence of exchange flow may destabilize an ascending gas slug and, vice versa, that the ascent of a gas slug may destabilize exchange flow. To test this hypothesis, we first investigate the dynamic interactions between exchange flow and slug ascent through analogue experiments, use these experimental results to ground-truth numerical simulations for the same setup, and then use the numerical simulations to generalize our laboratory findings.

Where within volcanic systems could exchange flow and slug ascent interact? Motivated by the relatively short time of 10-100 years that magma appears to reside beneath basaltic volcanoes (Pyle, 1992), Francis et al. (1993) argued for convective exchange between deep crustal reservoirs and the surface. At crustal depth, flow would be driven primarily by carbon dioxide, which is significantly less soluble in magma than water (e.g., Javoy & Pineau, 1991; Dixon et al., 1995) and exsolves well before the magma reaches the volcanic edifice (Métrich & Wallace, 2008). While exchange flow has been used to explain shallow degassing (Kazahaya et al., 1994), it is not necessarily limited to the shallow depth range, as illustrated in the conceptual sketch in Figure 1. Interactions between exchange flow and slug ascent could hence occur over the upper few kilometers of the plumbing system for deeply originating slugs as is the case, for example, at Stromboli volcano, Italy (Burton et al., 2007).

The ascent of a gas slug, or Taylor bubble, in initially stagnant liquid has been studied extensively in the laboratory as reviewed in the text book by Grace and Clift (1979). The ascent speed of the slug depends on whether inertial forces dominate over viscous and capillary forces (e.g., Dumitrescu, 1943; Davies & Taylor, 1950; White & Beardmore, 1962; R. Brown, 1965; Zukoski, 1966) as opposed to viscous forces dominating over inertial and capillary forces (e.g., Goldsmith & Mason, 1962; R. Brown, 1965; Wallis, 1969) or capillary forces dominating over viscous and inertial forces (e.g., Bretherton, 1961; Reinelt, 1987). Viana et al. (2003) compiled published data from 255 previous laboratory experiments, complemented by 7 new experiments, in an attempt to bridge these different regimes. Slug ascent has also been studied in the context of Poiseuille flow (Nicklin et al., 1962). Our work is the first attempt to combine slug ascent and exchange flow and assess whether the presence of a slug amplifies or reduces these potential instabilities.

The most common exchange-flow configuration for liquids with different viscosity in both laboratory experiments (Stevenson & Blake, 1998; Huppert & Hallworth, 2007;

Beckett et al., 2011) and numerical simulations (Suckale et al., 2018) is core-annular flow with the less dense liquid occupying the core and the more dense liquid descending in the outer annulus. For the laboratory portion of our study, we generate this flow field by using an experimental setup consisting of two reservoirs filled with unstably stratified liquid that are connected by a vertical glass pipe (see Figure 2). The setup mimics the experimental configuration of Beckett et al. (2011). We initiate core-annular flow by removing a rubber stopper at the top of the pipe connecting the two reservoirs and then inject gas slugs into the flow. We note that the evolving density stratification in the two reservoirs introduces a transient dynamics into the flow, but prior work shows that the flow profiles in the pipe closely approximate steady state (Beckett et al., 2011; Suckale et al., 2018).

There is no doubt that laboratory experiments have greatly advanced our understanding of the fluid dynamics contributing to eruptive processes in volcanic systems (Jaupart & Vergniolle, 1988; Seyfried & Freundt, 2000; James et al., 2006; Del Bello et al., 2015; J. Oppenheimer et al., 2020), but experimental insights are notoriously difficult to scale up to volcanic systems. Non-dimensional numbers can help attain greater generality, but laboratory experiments and volcanic systems are rarely, if ever, described by the exact same non-dimensional numbers, which would be required for scale invariance. This barrier is particularly pertinent for interface-dominated flows such as those considered here, because interface and body forces scale differently with spatial length, l (i.e., interface forces scale as l^2 and body forces as l^3). As a result, a change in spatial scale implies a change in the relative importance of interface to body forces. More specifically, interface forces tend to play a much larger role at laboratory as compared to volcanic scales.

To generalize our laboratory findings, we combine them with direct numerical simulations following the methodology of Qin and Suckale (2017). The advantage of direct numerical simulations is that they resolve the interactions between multiple different phases at the scale of individual interfaces (Suckale, Nave, & Hager, 2010; Qin et al., 2015; Qin & Suckale, 2017; Suckale et al., 2018), obviating the need for approximate parametrizations of drag, rise speed, or long-range hydrodynamic coupling. After reproducing the experimentally observed flow behavior to validate our numerical simulations, we can then investigate a broader range of parameters and behavior than is easily accessible in the laboratory. Despite this attempt to generalize, we emphasize that the primary focus of this study is to improve our process-based understanding of slug ascent in exchange flow.

The laboratory scale is uniquely suited for that specific purpose, providing a valuable stepping stone towards a more complete understanding of the dynamic interplay between exchange flow and slug ascent eventually.

2 Analogue laboratory experiments

We perform analogue laboratory experiments to better understand the dynamic coupling between exchange flow and slug ascent. Our work builds on previous experimental studies of exchange flow in a vertical pipe between two liquid reservoirs (Huppert & Hallworth, 2007; Beckett et al., 2011). We use an experimental setup that resembles that of Beckett et al. (2011), but additionally entails a rubber seal at the base of the pipe connecting the two liquid reservoirs to inject gas slugs into the flow. Figure 2 shows a diagram of the apparatus used. It consists of two 4.74 $\times 10^{-3}$ m^3 perspex reservoirs connected by a glass pipe of inner radius $R = 13.2$ mm and height $H = 1.00$ m. The top of the upper reservoir is open. The whole setup is attached to a steel frame which is mounted on adjustable legs to ensure the pipe is vertical.

The two reservoirs allow us to generate different background flows in the vertical pipe connecting the reservoirs. To study slug ascent in initially stagnant liquid, we fill both the lower reservoir and the pipe with the same liquid, golden syrup-water mixture. To generate unidirectional Poiseuille flow, we use the same setup but connect a hydraulic pump to the lower reservoir to pump liquid up through the apparatus at a constant volume flux. In contrast, core-annular-geometry exchange flow requires two different liquids that are initially unstably stratified. We fill the lower reservoir and pipe with a mixture of water and Golden Syrup (Tate and Lyle Ltd.), dyed red using food colouring. We then seal the top of the pipe (i.e., the base of the upper reservoir) with a rubber stopper and add pure Golden Syrup with higher density to the upper reservoir. We initiate core-annular flow by pulling the stopper up through the pure syrup and out the top of the apparatus with the aid of a thread.

The liquid properties for all experiments in the initially stagnant liquid and Poiseuille flow are summarized in Table 1 and for the core-annular flow in Table 2. We measured liquid viscosities using a Haake RV20 Rotational Rheometer with a Searle-type concentric cylinder system and calculated the liquid densities from calibration curves for Golden

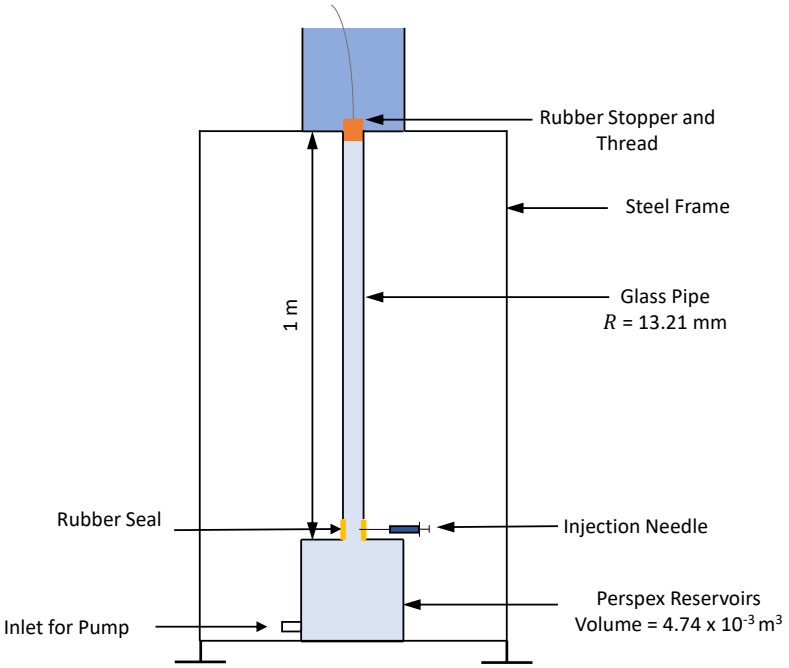

Figure 2. The experimental apparatus. As shown it is set up to generate an exchange flow by pulling up the stopper which initially separates the denser and more viscous liquid (darker blue) in the upper reservoirs from the less dense liquid in the pipe and lower reservoir (lighter blue). After the core-annular exchange flow became steady, a gas slug was injected through a rubber seal between the base of the pipe and the top of the lower reservoir. The inlet into the lower reservoir was used for experiments with a (unidirectional, upwards) background Poiseuille flow (with a single liquid).

Syrup and a wide range of Golden Syrup-water solutions relating density and viscosity (Beckett et al., 2011).

In all the experiments with an initially stagnant liquid, Poiseuille flow, and core-annular flow, gas slugs were injected through an annular rubber seal at the base of the pipe using a 50 ml syringe and 0.8 $\times$ 50 mm surgical needle. Only one slug was introduced to the flow at a time. We injected the slugs manually and the rate of injection was not controlled or measured, although subsequent modelling indicates that the rate of injection likely affects some results with core-annular background flow. We videoed the experiments and used Tracker image analysis software (D. Brown, Accessed 2011) to determine the vertical displacement of the front of the gas slug with time (see videos "Slug-Core-Annular-V-1", "Slug-Core-Annular-V-2" and "Slug-Core-Annular-V-3" in the on-

Table 1. Fluid properties and slug ascent speed in the initially stagnant liquid (U) and the Poiseuille flow (U_{P}). In this case, we define the aspect ratio, AR, as the ratio of slug length, l_s, to the pipe radius, R. The uncertainty in the liquid viscosity, μ, is $\sim 5\%$ in Pa s, and the liquid densities, ρ, have an uncertainty of ± 1 kg m^{-3}. The speed of the Poiseuille flow $\bar{U}_L$ is calculated from the known volume flux of the pump, which has an uncertainty of $\sim 1\%$. All velocities are in m s^{-1}.

Exp string	AR	μ	ρ	Eo	N_f	U	Re	$\bar{U}_L$	U_{P}
1p	5.8	49.5	1440	123	0.39	1.70E-3	0.001	4.21E-3	1.10E-2
2p	5.2	49.5	1440	123	0.39	1.70E-3	0.001	3.72E-3	9.47E-3
3p	5.2	49.5	1440	123	0.39	1.70E-3	0.001	4.03E-3	1.00E-2
4p	4.8	2.50	1393	119	7.49	3.05E-2	0.525	1.58E-3	3.31E-2
5p	4.6	2.30	1392	119	8.14	4.02E-2	0.615	2.87E-3	4.48E-2
6p	4.2	1.08	1381	118	17.2	7.17E-2	2.413	2.87E-3	7.63E-2
7p	3.8	0.623	1373	117	29.6	9.21E-2	5.896	2.87E-3	9.48E-1
8p	4.2	0.152	1352	116	120	1.50E-1	36.80	2.52E-3	1.53E-1
9p	3.8	0.127	1346	115	142	1.51E-1	44.78	2.36E-3	1.54E-1
10p	3.6	0.126	1349	115	144	1.53E-1	45.28	2.31E-3	1.58E-1
11p	3.8	0.0916	1342	115	197	1.54E-1	63.66	2.87E-3	1.59E-1
12p	3.4	0.0806	1339	114	223	1.57E-1	72.77	1.66E-3	1.60E-1
13p	3.2	0.0256	1326	113	696	1.60E-1	234.6	1.30E-3	1.62E-1

line supplement). Slug ascent speed was measured at distances $\geq 0.5H$ from the base of the pipe to ensure the slug has attained its terminal speed.

The experiments of gas slugs ascending through an initially stagnant liquid as well as a Poiseuille and core-annular flow have Reynolds numbers between 10^{-3} and 10^{2}. The Reynolds number captures the ratio of inertial to viscous forces

$$Re = \frac{\rho_f U L}{\mu_f} \ . \tag{1}$$

where U represents the slug ascent speed in an initially stagnant liquid, while ρ_f, L and μ_f are the density, width and viscosity of the liquid, f, that the slug rises through. In the initially stagnant liquid and the Poiseuille flow, there is only one liquid that fills the entire pipe and L is equal to the pipe diameter $2R$. In the case of the core-annular flow, we use the material properties of the core liquid to determine the Reynolds number and set L to the diameter of the core, $2R_c$, as determined by the analytical solution (Suckale et al., 2018).

In volcanic systems and in our laboratory experiments, it is difficult to estimate the Reynolds number a priori, because the characteristic speed, U is unknown a priori. We thus use the inverse viscosity, N_f, to characterize the nondimensional slug dynamics. The inverse viscosity differs from the Reynolds number only in assuming that the relevant characteristic velocity is the ascent speed of a slug in an initially stagnant liquid. It is defined as

$$N_f = \frac{(L^3 \rho_f^2 g)^{1/2}}{\mu_f} \ , \tag{2}$$

where g is the gravity. The range of N_f in the present work is $0.39 < N_f < 694$. Additionally, we use Eötvos numbers to present the ratio of inertia force to interfacial force, which is defined as,

$$Eo = \frac{\rho_f g L^2}{\sigma} \ , \tag{3}$$

where σ is the surface tension. In this study, we define σ as 0.08 N m^{-1} according to the surface tension of golden syrup (E. W. Llewellin et al., 2002). We do not expect the surface tension of the dilute syrup to differ significantly from that of pure golden syrup given that the surface tension of water is 0.07 N m^{-1}. Similar to the Reynolds number, we determine the inverse viscosity and Eötvos numbers of the core-annular flow using the properties of the core liquid. We list the values of the inverse viscosity and Eötvos numbers of our experiments for the initially stagnant liquid, the Poiseuille flow and the core-annular flow in Table 1 and Table 2, respectively.

Table 2. Fluid properties, and experimental measurements for gas slug ascent through the core-annular flow in a vertical pipe. The unit of the core liquid viscosity μ_c and annular liquid viscosity μ_a are Pa s. The density of the core liquid ρ_c and annular liquid ρ_a are in kg m^{-3}. The ascent slug increases the core radius, in m, from R_c to R_c'. In this case, we define the aspect ratio, AR, by dividing the slug length, l_s, to the core radius, R_c. The dimensionless numbers, Eo and N_f, are defined using the parameters of core liquid. The unit of both the averaged pure core speed $\bar{U}_L$ and slug ascent speed in the the core-annular flow U_{x} is m s^{-1}. The column "State" lists whether the slug was always stable (S) or experienced breakup (B) in the experiments.

Exp string	State	AR	μ_c	μ_a	ρ_c	ρ_a	R_c	R_c'	Eo	N_f	$\bar{U}_L$	U_{x}
1e	S	13.2	0.0845	52.2	1341	1438	5.6E-3	6.1E-3	20.2	58.1	3.82E-3	7.76E-2
2e	S	9.6	0.0200	65.2	1323	1442	4.8E-3	5.3E-3	14.7	192	1.30E-3	8.10E-2
3e	S	6.1	0.126	60.6	1349	1440	5.8E-3	6.4E-3	22.3	42.0	1.60E-3	6.08E-2
4e	B	-	0.0776	64	1343	1441	5.0E-3	-	16.6	54.5	-	-
5e	B	-	0.151	65.4	1352	1442	5.6E-3	-	20.4	32.5	-	-
6e	B	-	0.175	60.3	1354	1440	-	-	-	-	-	-
7e	B	-	0.0806	54.3	1340	1441	-	-	-	-	-	-

3 Numerical Simulations

In our simulations, we only model the flow in the vertical pipe connecting the two reservoirs, but not the flow in the reservoirs. Instead, we can enforce the three different flow fields through the boundary conditions. The advantage of this approach is that it eliminates the transient dynamics associated with the gradual draining of the two reservoirs over time and ensures steady-state conditions. Assuming axisymmetry in the flow, we reduce the three-dimensional problem to a quasi-two-dimensional computation with a symmetry boundary condition in the center of the pipe, as illustrated in Figure 3.

3.1 Governing Equations

We solve for conservation of momentum and mass in incompressible flow,

$$\nabla \cdot \mathbf{v} = 0 \ , \tag{4}$$

$$\rho \left(\frac{\partial \mathbf{v}}{\partial t} + (\mathbf{v} \cdot \nabla)\mathbf{v} \right) = -\nabla p + \nabla \cdot \left[\mu(\nabla \mathbf{v} + (\nabla \mathbf{v})^T) \right] + \rho \mathbf{g} \ . \tag{5}$$

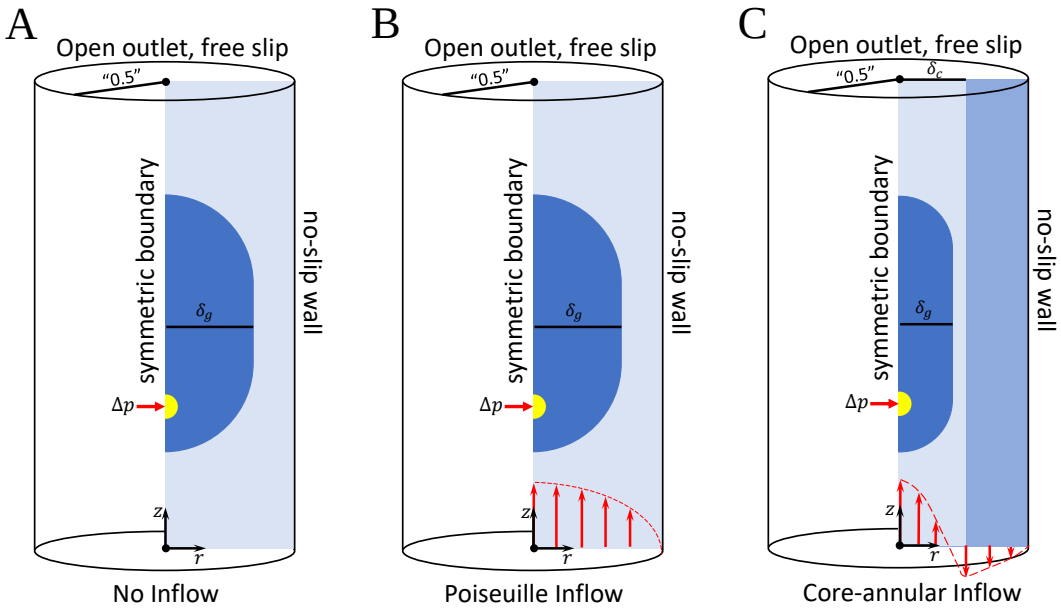

Figure 3. Setup of the 2-D axisymmetrical numerical simulations for a gas slug (dark blue) ascending through the three different flow fields considered. The model domain is not shown to scale. A. In an initially stagnant liquid (light blue), there is no inflow at the lower boundary; B. Poiseuille flow (light blue) is driven by a parabolic velocity profile at the lower boundary; C. Core-annular flow requires two liquids, the core liquid (light blue) and the annulus liquid (intermediate blue). In all three models, the slug is injected by applying an elevated pressure, Δp, at a small spherical region at the inner boundary (marked in yellow).

where $\mathbf{v}$ is the velocity, p the pressure, $\mathbf{g}$ the gravitational acceleration, ρ and μ are the density and viscosity.

Density and viscosity represent individual phase properties that change discontinuously and often dramatically at the interface. For example, the viscosity changes discontinuously at the phase boundary between fluid and gas,

$$\mu(\mathbf{x}) = \begin{cases} \mu_g & \text{in the gas slug} \\ \mu_l & \text{in the liquid} \end{cases}, \tag{6}$$

where μ_g and μ_l are the gas and liquid viscosity, respectively. In the core-annular flow with ascending slug, the viscosity profile is,

$$\mu(\mathbf{x}) = \begin{cases} \mu_g & \text{in the gas slug} \\ \mu_c & \text{in the core flow} \\ \mu_a & \text{in the annular flow} \end{cases}, \tag{7}$$

where μ_g represents the gas viscosity in core-annular flow, and μ_c and μ_a are the viscosity of core and annular liquids, respectively. In the present work, we assume that all phases, including liquids and the gas, abide by a Newtonian rheology.

Three different phases are present in the core-annular flow, implying the need to track two interfaces, the gas-liquid interface delineating the gas slug and the liquid-liquid interfaces separating the ascending and descending liquids. In the numerical simulation, we advect the interfaces separately with the flow field according to

$$\frac{\partial \Gamma_i}{\partial t} + (\mathbf{v} \cdot \nabla)\Gamma_i = 0 \ , \tag{8}$$

where the subscript, i, indicates the phase interface, $i =$ "gl" for the gas-liquid interface while $i =$ "ll" for the liquid-liquid interface. During slug ascent through an initially stagnant liquid and in Poiseuille flow, we only have the gas-liquid interface, so that there is only $i =$ "gl".

Independent of the flow field, the jump condition of the normal stress across an interface, Γ_i, combines the effect of the surface tension and stress,

$$[\,p\,]_{I_i} = \sigma_i \kappa_i + 2[\mu]_{I_i}\, \mathbf{n}_i^T \cdot \nabla \mathbf{v} \cdot \mathbf{n}_i \, , \tag{9}$$

where $[\,\cdot\,]_{I_i}$ indicates the sharp jump across the interface, κ_i is the interface curvature, $\mathbf{n}_i$ is the normal vector of the interface, and σ_i is the surface tension. In this work, we set the surface tension on gas-liquid interface as $\sigma_{gl} = 0.08$ N m^{-1} (E. W. Llewellin et al., 2002), and assume there is no surface tension on the liquid-liquid interface.

To non-dimensionalize our governing equations (Eqs. 4-5), we define the following non-dimensional quantities

$$\mathbf{x}^* = \frac{\mathbf{x}}{L}, \mathbf{v}^* = \frac{\mathbf{v}}{U}, t^* = \frac{t}{L/U}, p^* = \frac{p}{\rho_f U^2}, \rho^* = \frac{\rho(\mathbf{x})}{\rho_f}, \mu^* = \frac{\mu(\mathbf{x})}{\mu_f} \tag{10}$$

where the parameter L, U, ρ_f and μ_f are identical to the definitions in Section 2. We substitute Eq. 10 into Eqs. 4-5, rearrange, and drop the stars, obtaining the governing equations in non-dimensional form,

$$\nabla \cdot \mathbf{v} = 0 \ , \tag{11}$$

$$\frac{\partial \mathbf{v}}{\partial t} + (\mathbf{v} \cdot \nabla)\mathbf{v} = -\frac{\nabla p}{\rho} + \frac{1}{Re\,\rho} \nabla \cdot \left[\mu(\nabla \mathbf{v} + (\nabla \mathbf{v})^T)\right] + \frac{1}{Fr}\mathbf{z} \ , \tag{12}$$

where Re represents Reynolds number (Eq. 1) and Fr represents Froude number, $Fr = \frac{U}{\sqrt{gL}}$.

3.2 Boundary and Initial conditions

In our simulations, we enforce the three different flow fields representing the initially stagnant liquid, Poiseuille flow and core-annular flow through the boundary conditions. In the case of the initially stagnant liquid (Figure 3A), we apply zero inflow condition to the bottom of the computational domain. At the top boundary, we impose open outflow by enforcing constant pressure, p_t=const, and free stress, $\partial \mathbf{v}/\partial z|_t$=0. We treat the outer pipe as a no-slip wall, where $\mathbf{v}_w = 0$, and $\partial p/\partial \mathbf{n}|_w$=0, with $\mathbf{n}_w$ the unit vector normal to the wall. At the symmetric boundary at the center of the pipe, we apply a free-slip boundary, as $\partial \mathbf{v}/\partial \mathbf{n}|_s = 0$, and $\partial p/\partial \mathbf{n}|_s$=0, with $\mathbf{n}_s$ the unit vector normal to the symmetric boundary.

Our simulations for the case of a Poiseuille flow and core-annular flow employ the same boundary conditions, except for the boundary condition at the bottom of the computational domain. To generate Poiseuille flow (Figure 3B), we set the inflow at the bottom of the computational domain to be a parabolic velocity profile as,

$$u_b = 2\hat{U}_L(1-(2r)^2) \tag{13}$$

where r ($\in [0, 0.5]$) represents the dimensionless radial coordinate and $\hat{U}_L$ is the dimensionless, average speed. We define $\hat{U}_L$ as $\hat{U}_L = \bar{U}_L/U$, where $\bar{U}_L$ is the known volume flux of the pump used in the experiments.

Modeling exchange flow requires two separate liquids illustrated in light and intermediate blue (Figure 3C). The presence of an additional interface complicates the boundary conditions slightly, because it requires enforcing not only the flow field itself but also the position of the liquid-liquid interface. We define the inflow profile based on the experimentally measured half core thickness, δ, non-dimensionalized by the pipe diameter and use the analytical model proposed by Suckale et al. (2018) for the dimensionless speed profiles in the core (u_c) and annulus (u_a),

$$u_c(r) = \frac{M(P-1)}{\alpha}(r^2-\delta^2)+u_i, \qquad r\in[0,\delta] \tag{14}$$

$$u_a(r) = \frac{1}{\alpha}\left[\frac{P}{4}(4r^2-1)-2\delta^2\log(2r)\right], \quad r\in[\delta,0.5] \tag{15}$$

where α is the ratio of the velocity scale used in the present work, U, to the velocity scale used by Suckale et al. (2018), $(\rho_a-\rho_c)gR^2/\mu_a$, $M=\mu_a/\mu_c$ is the viscosity ratio, P is

the non-dimensional pressure drop driving the descending phase, defined as,

$$P = 4\delta^2 \frac{2(4\delta^2 - 1) - 4M\delta^2}{(16\delta^4 - 1) - 16M\delta^4} \ , \tag{16}$$

and $u_i = u_a(\delta) = u_c(\delta)$ is the vertical flow speed at the interface given by

$$u_i = \frac{1}{\alpha}\left[\frac{P}{4}(4\delta^2 - 1) - 2\delta^2 \log(2\delta)\right]. \tag{17}$$

In all of our simulations, we assume that only the thick-core solution is realized since it is most commonly observed in experiments (Stevenson & Blake, 1998; Picchi et al., 2020).

At the beginning of all simulations, we mimic the experimental injection of a gas slug by applying an additional injection pressure term to the momentum equation (Equation 5) inside a small, semi-spherical region (highlighted in yellow in Figure 3 A-C). The injection region includes a portion of the boundary in the center of the pipe. We apply an elevated pressure until the the slug volume is comparable to the one used in the experiments. To prevent the slug from touching the lower boundary, we inject the slug at a finite height above the bottom boundary. We set this height to 1/8 of the whole domain length.

3.3 Numerical method

We build our numerical model based on the computational techniques that are derived, verified and validated by Qin and Suckale (2017) and Qin et al. (2020). Our approach is optimized for modeling multiphase flow in volcanic systems, where large contrasts in density and viscosity are common. Our numerical approach includes three main components. The first component is a 2D axisymmetric multiphase Navier-Stokes solver proposed by Qin et al. (2020), which discretizes the governing equations 4-5 through the structured Marker And Cell method (Harlow & Welch, 1965). The velocity vector field, $\mathbf{v}$, is defined at the grid-cell faces, and the scalar fields (e.g., p, ρ, μ) are defined at the grid-cell centers. To maintain the accuracy and efficiency of the numerical solution, we employ an implicit implementation of the viscous term, a time-step splitting approach, and an approximate factorization of the sparse coefficient matrices (Kim & Moin, 1985).

The second key component of our computational technique is a level-set-based interface solver capturing the advection of the gas-liquid and liquid-liquid interfaces through a topology preserving strategy (Qin et al., 2015). Here, we include up to three fluids, i.e., the gas slug, the core liquid, and the annular liquid. We hence need up to two level set

functions, ϕ_i, to represent the gas-liquid interface, Γ_{gl}, and the liquid-liquid interface, Γ_{ll}). These two interfaces divide the domain into three fluids. In the simulation, we advect ϕ_{gl} and ϕ_{ll} separately by solving the following equation,

$$\frac{\partial \phi_i}{\partial t} + (\mathbf{v} \cdot \nabla)\phi_i = 0 \ . \tag{18}$$

We redistance the two level sets separately through the geometry projection scheme introduced by Qin et al. (2015).

The third component is the ghost-fluid method used to capture the jump condition across the interface (Equation 9) proposed by Kang et al. (2000). We assume that there is no surface tension at the liquid-liquid interface and smooth the viscosity profile around the interface over two grid cells, following previous studies (e.g., Sussman et al., 1999; Olsson & Kreiss, 2005; Qin & Suckale, 2017). This approach is equivalent to neglecting any jumps that could occur at the liquid-liquid interface. We only apply the ghost-fluid method to capture the jump condition across the gas-liquid interface, which is caused primarily by surface tension.

3.4 Verification and Validation

We verify and validate our numerical model, as well as the experimental methodology, by comparing our results to existing theoretical solutions and empirical correlations as described in detail in the supplementary material. To evaluate our ability to capture the slug ascent speed in the initially stagnant liquid, we compare our experimental measurements, U_s (Table 1), and the corresponding numerical reproduction to the analytical solution given by Picchi et al. (2020) and the empirical speeds proposed by Viana et al. (2003). We also use a theoretical relationship between the slug ascent speed and the ambient flow, given by Nicklin et al. (1962), to validate our ability to predict the effect of the ambient flow on the ascent of the slug. The results from our verification and validation analysis in the supplementary material indicate that our simulations are in good agreement with previous analytical and empirical solutions.

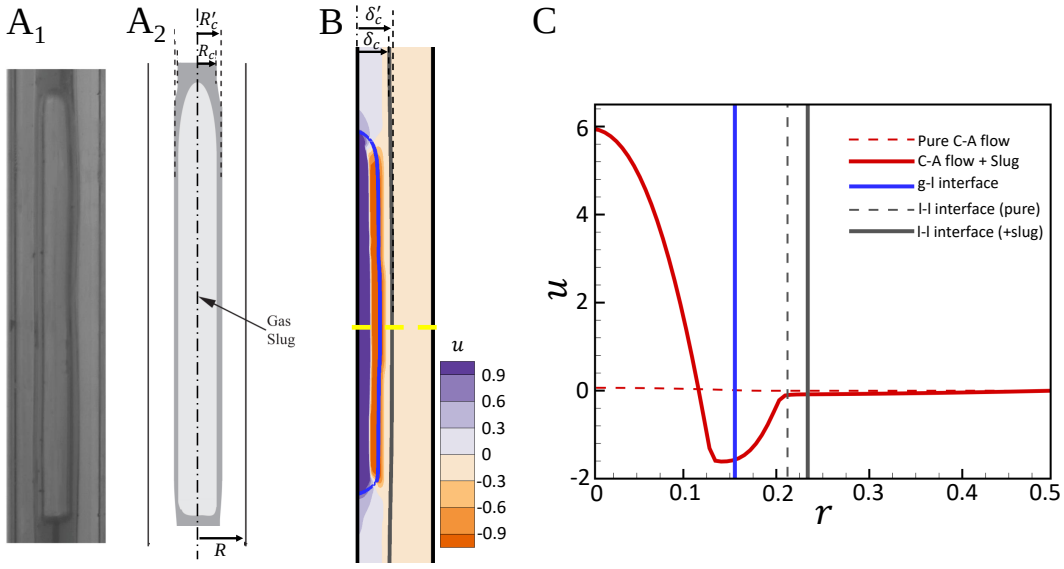

Figure 4. The effect of a single, stably ascending slug on core-annular flow. A_1: Photo of experiment 3e showing gas slug ascent through core annular flow. A_2: A sketch of A_1 presenting the ascent slug increases the core radius from R_c to R_c'. B: Snapshot of the numerical reproduction of experiment 3e, showing the core radius increased from $\delta_c = 0.22$ to $\delta_c' = 0.24$. The color scale represents the magnitude of the vertical speed. C: Horizontal profile of the vertical speed at the cross section marked by yellow dashed line in plot B. The blue line shows the gas-liquid interface, while the gray dashed and gray solid lines represent the liquid-liquid interface without and with a slug, respectively. For comparison purposes, we plot the speed profile of the core-annular (abbreviated as C-A) flow prior to the introduction of gas slug as a red dashed line.

4 Results

4.1 The effect of core-annular flow on slug ascent

A slug ascending through core-annular flow alters the ambient flow pattern, because it has to displace fluid to move. At the same time, the slug ascent speed is altered by the ambient, non-zero flow speed. To discuss our results regarding the interaction between a slug and its surrounding core-annular flow, we focus primarily on experiment 3e and its numerical reproduction in this section. The other experiments with stable slugs, experiments 1e and 2e, are consistent with the behavior in experiment 3e and are included in the supplementary material (Section S4).

We observe that the gas slug always ascends in the core flow, regardless of whether it was originally injected into the core or the annulus. In addition to the speed being upwards-oriented, the viscosity in the core is lower, reducing the work required for slug ascent. As shown in Figures 4, the ascending slug in experiment 3e slightly widens the core flow (Figures 4 A_1 and A_2), increasing the core radius, R_c, by about 10% to R_c' (see Table 2). Videos "Slug-Core-Annular-V-1" and "Slug-Core-Annular-V-3" available as supplementary material also show examples of slug ascent with different slug length. Our numerical simulation, based on gas injected at $\Delta p = 10$ in $r_{\Delta p} = 0.2$, agrees well with the experimental observation (Figure 4 B). However, in both the experiment and the numerical simulation, the widening is only local and the core thickness above and below the slug remain approximately equal to the thickness of the core in the absence of a slug.

Figure 4 B also illustrates the effect of an ascending slug on the dynamics of the core-annular flow. Since the ascent speed of the slug is much faster than that of the core flow in the absence of the slug, the two flows are largely decoupled. The color scale in Figure 4 B illustrates the notable difference in the two speeds. Figure 4 C compares the velocity profile at the cross section located in the middle of the slug to the flow profile prior to the introduction of the slug. The background flow is almost stagnant in comparison to the flow speed created by the ascending slug.

In Figure 5, we plot the dimensionless slug ascent speeds, $\hat{U}$, measured in our experiments and simulations, versus the dimensionless average speed of pure core flow, $\hat{U}_c$. All speeds are non-dimensionalized by the slug ascent speed in an initially stagnant liquid, which is calculated from the Fr predicted by the correlation given by Viana et al. (2003) (see equation (S2) in the supplementary material), with the characteristic length, L, defined as pure core diameter before the slug pass through, $2R_c$. Figure 5 demonstrates that the relationship between slug ascent speed and core speed is well described by $\hat{U}=2\hat{U}_c+1$. This finding implies that the theoretical correlation originally derived by Nicklin et al. (1962) for slugs ascending in Poiseuille flow can be generalized to core annular flow by using the core radius in place of the tube radius.

4.2 Stability of the injected slug

In experiments 1e, 2e, and 3e, the injected gas volume formed a stable slug interface, reminiscent of slugs ascending in initially stagnant liquid. In some cases (i.e., ex-

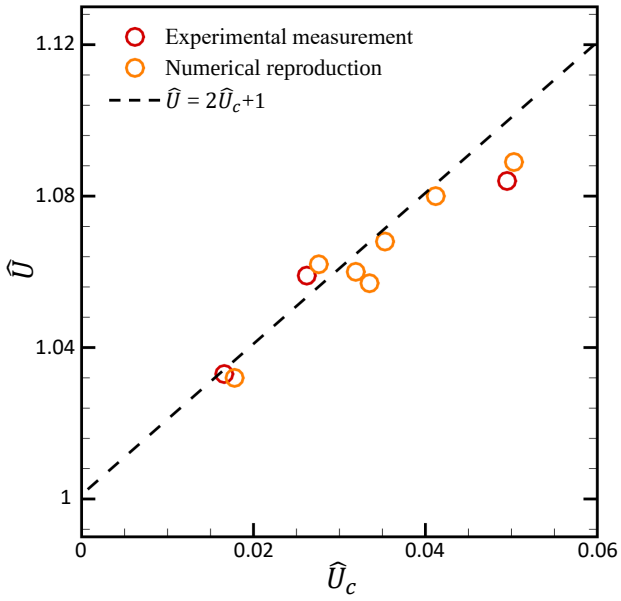

Figure 5. Normalised ascent speed of a single gas slug through the core-annular flow. The dashed line represents the theoretical correlation, $\hat{U} = 2\hat{U}_c + 1$. Red circles represent the experimental data, while yellow circles represent the numerical data.

periments 4e-5e), however, the injected gas volume forms a slug that becomes unstable shortly after injection and breaks up, as illustrated in Figure 6 A. For the experiments with unstable slugs, it is hence not possible to measure a single slug ascent speed. Interestingly, slug instability only arises in experiments with core-annular flow. We have not observed similar instabilities in the experiments injecting gas into an initially stagnant liquid or Poiseuille flow.

We hypothesize that the slug instability observed in some core-annular flow experiments is a result of the gas injection method. To test this hypothesis, we numerically reproduce the slug instability in Figure 6 B1-B3 using the parameters of experiment 4e. In the simulation, we inject the gas slug into the core flow by applying a high injection pressure, $\Delta p = 10^4$, into the injection region. The radius of the computational injection region is identical to the needle used in the experiments, $r_{\Delta p} = 0.035$. The high pressure Δp leads to a large volume of gas suddenly displacing the core liquid. The gas-liquid interface extends rapidly and disturbs the liquid-liquid interface. The interaction between the two interfaces deforms the liquid-liquid interface, as shown in Figure 6 B_1. After injection, the deformed liquid-liquid interface gradually retracts to a smoother shape,

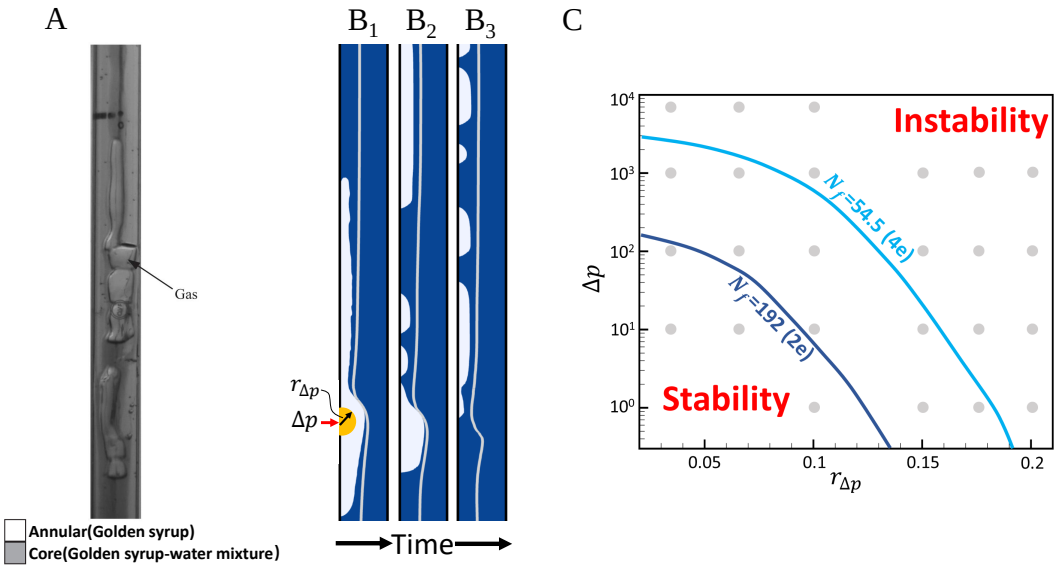

Figure 6. A: Photo of experiment 4e in which a single gas slug breaks up during ascent. B_1-B_3: Numerical reproduction of the break-up observed in experiment 4e, highlighting how the excess gas volume bends the liquid-liquid interface (B_1) and affects slug break-up (B_2-B_3). C: Regime diagram for the instability caused by the mechanism of gas injection, where two major factors, pressure difference and the radius of the injection region, are plotted against each other. The gray circles mark the numerical simulations we performed. The blue lines indicate how the regime of stability increases as the inverse viscosity N_f decreases, based on experiments 2e and 4e.

but adjusts more slowly than the gas-liquid interface, creating a sustained perturbation to the slug. In the process, the ascending slug breaks up into multiple small blobs (Figure 6 B_2-B_3). Similar to the experiments, the gas phase in our simulations never crosses the liquid-liquid interface. Instead, the gas remains entrained in the core flow.

In addition to the injection pressure Δp, our simulations show that the radius of the injection region, $r_{\Delta p}$, plays an important role in controlling the stability of the injected slug. The closer the boundary of the injection region to the liquid-liquid interface, the more the two interfaces interact with each other and the higher the tendency for instability. We summarize the effect of Δp and $r_{\Delta p}$ on the stability of the injected slug in Figure 6 C. At a given inverse viscosity, N_f, there is a critical injection pressure above which the instability shown in Figure 6 B_1-B_3 occurs, and this critical injection pressure decreases with the radius of the injection region. The comparison between the curves sep-

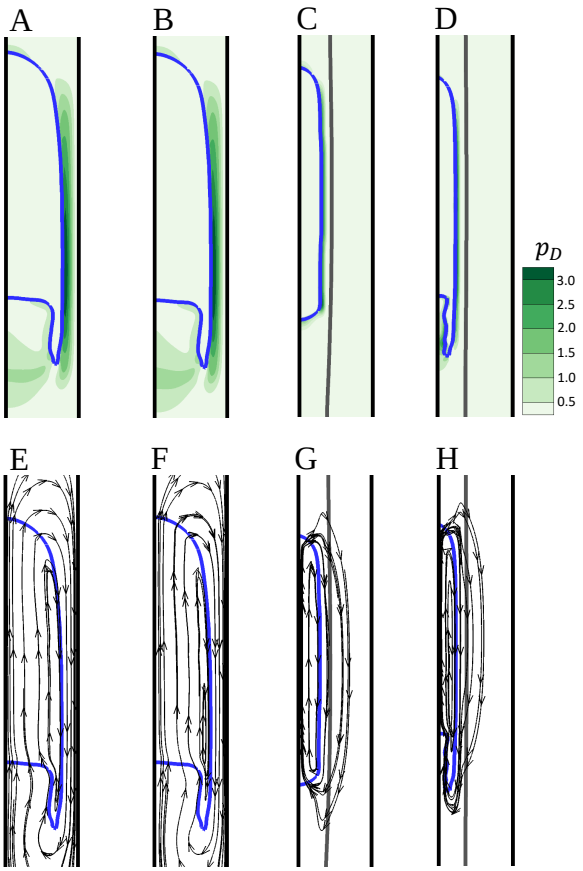

Figure 7. Comparison of the slug shape, dynamic pressure and streamlines during ascent through an initially stagnant liquid (A/E), Poiseuille flow (B/F) and core-annular flow (C/G) and (D/H). In (C/G), the properties of the core liquid is same as the liquid properties in (A/E) and (B/F). In (D/H), the inverse viscosity, N_f, is same as the one of (A/E) and (B/F). The color scale in plots A-D represents the dimensionless dynamic pressure, while the arrow lines in E-H represent the streamlines.

arating the stability and instability regimes for different N_f suggests that the sensitivity of the instability to the injection mechanism varies with the liquid properties.

Given a suitable injection process, however, the stability of gas slugs in core-annular flow is comparable to gas slugs rising in an initially stagnant liquid or in Poiseuille flow with matching non-dimensional conditions as demonstrated in Figure 7. We compare slug ascent in an initially stagnant liquid (Figures 7A/E) and Poiseuille flow (Figures 7B/F) using the properties of experiment 12p (Table 1) to core-annular flow (Figure 7C/G) using the properties of experiment 7e (Table 2) for which the slug injection process was

stable. The properties of the liquid in Figures 7A-B are the same as the properties of the core liquid in the core-annular flow in in Figure 7C. We set the initial slug length to be equal in all simulations, as shown in Figure 7.

We find that the slugs in the initially stagnant liquid and the Poiseuille flow develop a similar shape (Figures 7A-B), characterized by stretched out tails at the rear of the slug. In contrast, the slug in the core-annular flow develops a blunt shape at both head and tail (Figures 7C/G). This blunt shape is a result of the slug rising through a slightly narrower domain, the core, which reduces the inverse viscosity N_f. The color scale represents the dimensionless dynamic pressure, defined as $p_D = \frac{1}{2}\rho|\mathbf{v}|^2$. An asymmetric deformation of the slug, indicative of the onset of inertia-related nonlinearity in the flow, appears in core-annular flow only (see Figures 7D/H) after reducing the core liquid viscosity slightly such that N_f is the same as in the initially stagnant liquid and the Poiseuille flow (Figures 7A/E and B/F).We conclude that slug instability is governed primarily by N_f rather than by the nature of the background flow field.

4.3 The effect of slug ascent on core-annular flow

A characteristic of stable core-annular flow is that the flux in the core is balanced by the flux in the annulus, creating zero net flux. Slug ascent perturbs this flux balance, because it forces the core liquid in the immediate vicinity of the slug to flow downwards instead of upwards. At first sight, one might expect the conduit-wide effect of this localized switch in flow direction to be negligible, because only a small portion of the core liquid is affected by it, but the ascent speed of the slug is much larger than the average ascent speed of the core liquid. As a consequence, the forced, rapid downwards motion of the core liquid around the slug could significantly alter the overall flux balance. This effect would be amplified if multiple slugs rise in succession rather than in isolation as could be the case in some volcanic systems (Pering et al., 2017).

To better understand potential new instabilities arising from the joint presence of both slug ascent and core-annular flow in volcanic systems, we study the effect of multiple slugs on core-annular flow. To introduce multiple slugs, we generalize the injection mechanism used in our experiments. Using the same injection zone and pressure (see section 3.2), we introduce multiple slugs at a constant injection frequency, f, where we define injection frequency as the ratio of the slug ascent speed to the domain length divided

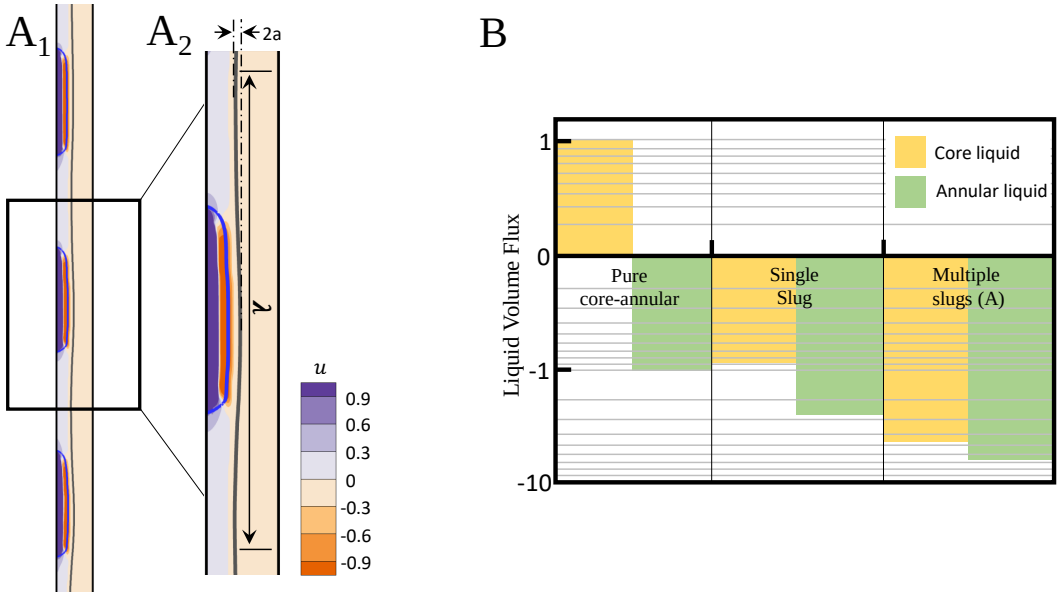

Figure 8. A1: Snapshot of a numerical simulation for the core-annular flow involving multiply injected slugs. A2: Zoom-in image of A1 presenting the wave-formed liquid-liquid interface, caused by ascent of slugs, whose peak-to-peak amplitude is $2a$ and wave length is λ. B: Comparison of the volume flux of the liquids in pure core-annular flow and core-annular flow with a single or multiple slugs of the same size injected into it. All the volume fluxes are averaged over the domain length.

by the number of slugs. We maintain the same boundary conditions as in our simulations of single slugs ascending. We use the material properties from experiment 3e as an example and inject each slug at $\Delta p = 10$ in $r_{\Delta p} = 0.2$.

We quantify the effect of sequential slug ascent on core-annular flow by comparing the liquid volume fluxes in the core and annulus. We compute the liquid flux of the core flow, F_c, at each cross section by integrating in the radial direction

$$F_c = \int_{\delta_g}^{\delta_c} 2\pi r u(r) \mathrm{d}r \approx \sum^{N_c} 2\pi r_i u_{i,J} \Delta r \ , \ i = \{(1, ..., nx) : (\phi_{ll})_{i,J} < 0 \ , \ (\phi_{gl})_{i,J} > 0\} \ , \quad (19)$$

where δ_g and δ_c are the dimensionless thickness of gas region and the core flow, respectively. The variable N_c is the number of discrete grids in the core liquid at an arbitrary vertical coordinate, J. In the computation of N_c, we consider only the grid cells where the level set function, ϕ_{gl}, is positive. The variables r_i and $u_{i,J}$ represent the width and vertical speed on the discrete grids at J, Δr is the grid size in r component of the axisymmetric coordinate. Similarly, we compute the liquid flux of the annular flow, F_a, at

each cross section by evaluating,

$$F_a = \int_{\delta_c}^{0.5} 2\pi r u(r) \mathrm{d}r \approx \sum^{N_a} 2\pi r_i u_{i,J} \Delta r \ , \ i = \{(1, ..., nx) : (\phi_{ll})_{i,J} > 0 \ , \ (\phi_{gl})_{i,J} > 0\} \ , \quad (20)$$

where N_a is the number of discrete grids inside the annular liquid at an arbitrary vertical coordinate, J.

Figures 8 A_1-A_2 present snapshots of a simulation with multiple slugs injected at a frequency of 0.69 Hz. The presence of the slugs creates a wave-like perturbation on the exchange-flow interface. The wavelength depends on the injection frequency and the length of each slug. The peak-to-peak amplitude of the wave, $2a$, equals approximately the increase in core-thickness generated by a single slug, $\delta_c' - \delta_c$, shown in Figure 4, suggesting that each slug ascends independently. Figure 8 B shows the results of the flux computation on a logarithmic scale. We average the liquid fluxes computed from Eqs. 19-20 over the computational domain shown in A1 and over time. We non-dimensionalize all liquid fluxes by the core liquid flux of the pure core-annular flow computed using the speed profile (Eq. 14) from Suckale et al. (2018). It is striking that only pure core-annular flow is associated with a stable flux balance (Figure 8 B). In pure core-annular flow, the flux in the core is equal to the flux in the annulus, but has a different sign since it is oriented in the opposite direction. Using the properties of experiment 3e, the core and annular liquid fluxes of the pure core-annular flow are 1.35×10^{-3} and -1.35×10^{-3}.

Our simulations suggest that even the passage of a single slug can temporarily shift the flux balance of pure core-annular flow to downwards in both liquids. The perturbation introduced by a single slug is transient and short-lived, partly because the passage of the slug is relatively fast. The core-annular flow recovers, avoiding the buildup of liquid at depth and instability. Multiple slugs create a lasting disruption with the downwards flux in the core liquid being about three-fold higher than for a single slug, because in this specific simulation three slugs ascend simultaneously in the computational domain. Interestingly, slug ascent in the core liquid also entails speed-up of the downwards-oriented flux in the annulus (see green bars in Figure 8 B), amplifying the flux imbalance.

Figure 9 summarizes in more detail how the liquid fluxes in the core and annulus depend on slug length (plot A), injection frequency (plot B), the number of slugs at a fixed gas volume ratio (plot C) and inverse viscosity (plot D). These liquid fluxes are computed in domains where slugs ascend throughout, like the one shown in Figure 8 A_1. We

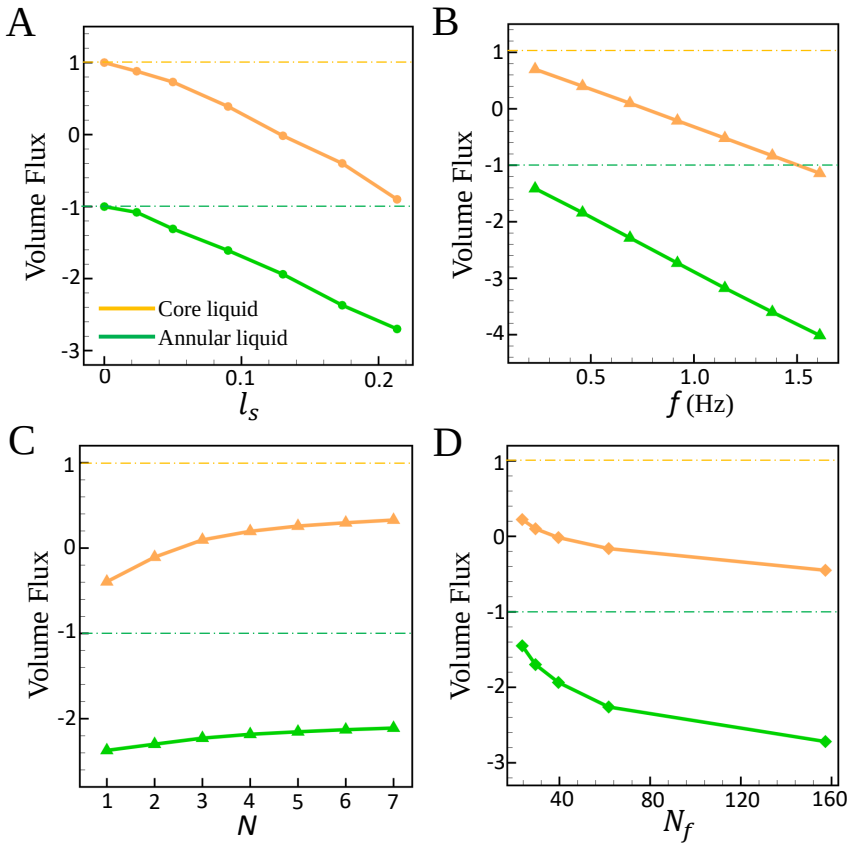

Figure 9. A: Variation of core and annular liquid volume flux with the length of a single slug, non-dimensionalized by the domain length. B: Dependence of the volume flux in the core and annulus on injection frequency for a constant non-dimensional slug length of 0.05. C: Dependence of core and annular liquid volume flux on number of slugs for a fixed gas volume to core liquid volume ratio of 0.1. The properties used in A, B and C are the same as those in experiment 3e. D: Dependence of the volume flux in the core and annulus on inverse viscosity, N_f, for an injection frequency of 0.23 Hz and a slug length of 0.12. Dashed lines mark the volume flux for a balanced exchange flow without slugs.

find that at a constant injection frequency (e.g., $f = 0.23$ Hz), the core flux switches from positive to negative already for relatively small slugs (e.g., with the slug length non-dimensionalized by the domain length, l_s, of 0.12). With increasing slug length, the imbalance of fluxes increases. The injection frequency has a similar effect on the liquid fluxes. For constant slug length, the imbalance of fluxes increases almost linearly with the injection frequency (see Figure 9 B), suggesting that each slug ascends independently, as shown in Figure 8 A_1. The approximately linear relationship between the injection frequency and the liq-

uid flux is consistent with the results in Figure 8 B, where three slugs create a three-fold higher disruption in the core flux than a single slug.

At the same total gas volume, a large number of small slugs tends to be less disruptive than a small number of large slugs, but the effect is small. Figure 9 C shows that for a fixed volume ratio (10%) of gas to core liquid, increasing the number of slugs decreases the imbalance of fluxes. This result is consistent with the velocity field shown in Figure 8 A_2, where the slug promotes upward flow around the head and tail, but forces downward flow along its side. At fixed volume ratio of gas to core liquid, multiple short slugs provide more heads and tails than a single long slug, creating relatively more upward-oriented flow areas and a smaller flux imbalance. We also find that the viscosity of the core liquid has a significant effect on the flux imbalance (see Figure 9 D). Lower viscosity implies smaller viscous forces. As a result, the liquid fluxes increase in both core and annulus with the inverse viscosity when the slug length and injection frequency are constant.

5 Implications for understanding persistently active volcanoes

Persistently active volcanoes exhibit a stunning diversity in eruptive behavior. Existing conceptualizations associate eruptive regimes with established flow regimes in two-phase pipe flow: Bubbly flow is associated with passive degassing, slug flow with Strombolian-type eruptions and churn flow with Hawaiian activity (Wilson, 1980; Vergniolle & Jaupart, 1986; Jaupart & Vergniolle, 1988; E. Parfitt & Wilson, 1995; E. A. Parfitt, 2004; James et al., 2009; Fowler & Robinson, 2018). Within this framework, eruptive regimes represent separate non-dimensional regimes with transitions arising if there is a system-scale change, such as an elevated influx of gas or magma from depth. Our results suggest that regime transitions could also occur as a consequence of the dynamic interplay between slug ascent and exchange flow in the conduits of persistently active volcanoes.

Our experiments indicate a wide spectrum of behavior, from stable slug ascent reminiscent of that seen in an initially stagnant liquid (see Section 4.1) to slug breakup as a consequence of the dynamic interactions between the slug- and the exchange-flow interface (see Section 4.2), and, finally, exchange-flow destabilization due to the ascent of multiple slugs (see Section 4.3). These observations highlight the wide range of possible interactions that exist, even in a highly idealized laboratory setting. In volcanic sys-

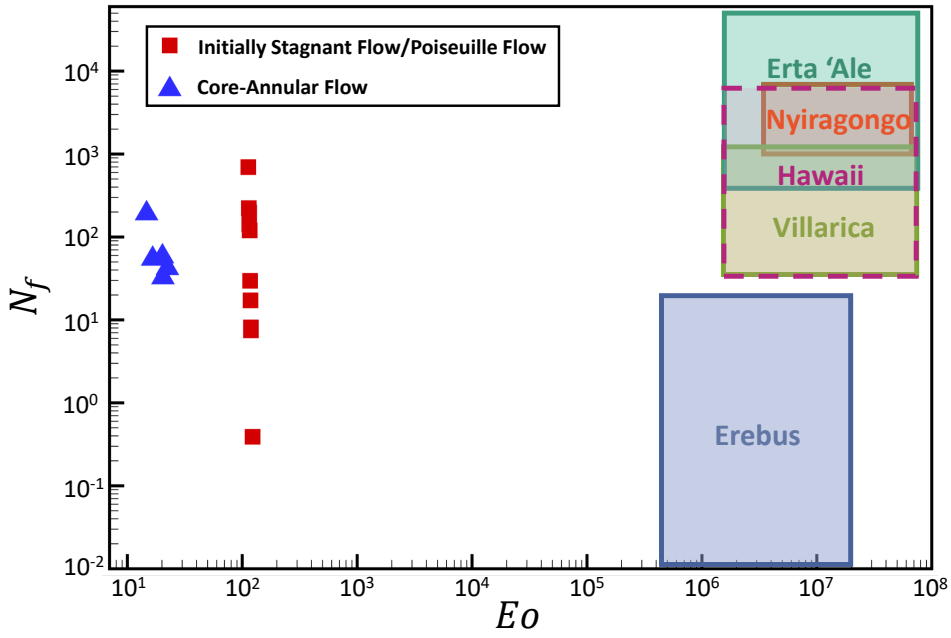

Figure 10. Non-dimensional conditions captured in our laboratory experiments in comparison to several persistently active volcanoes.

tems, many additional factors, not considered here, could amplify these interactions, including decompression (James et al., 2004, 2008; Del Bello et al., 2012; Allard, 2010), crystallization (Del Bello et al., 2015; Suckale et al., 2016; J. Oppenheimer et al., 2020), depth variability in gas content or magma properties (Massol et al., 2001; Melnik & Sparks, 2005; Collier & Neuberg, 2006; Capponi et al., 2016), complex conduit geometries (James et al., 2006; Costa, Melnik, Sparks, & Voight, 2007; Vitturi et al., 2008), and deformation of the volcanic edifice (Maeda, 2000; Barmin et al., 2002; Costa, Melnik, & Sparks, 2007).

To provide a first step towards a more complete understanding of the flow conditions in the conduits of persistently active volcanoes, we focus on the laboratory scale, which is uniquely well suited to advance our process-based understanding of conduit flow. The non-dimensional regime covered in our experiments is motivated by volcanic systems and covers both the viscous-dominated regime and flows where inertial effects become important (see Figure 10). We emphasize that we only obtain reasonable overlap in terms of the ratio between inertial and viscous forces captured through the inverse viscosity. In contrast, the Eötvös number differs by several orders of magnitude, suggesting that surface tension and other interfaces forces are significantly more pronounced in

our experiments than they would be in actual volcanic systems. We note that this issue is common in analogue experiments of slug ascent aimed at understanding volcanic systems (James et al., 2004, 2006, 2008; E. Llewellin et al., 2012), because of the different scaling properties of interfaces and body forces. Also, to demonstrate the capability to generalize to volcano-specific conditions, we have performed a simulation specifically for Erebus and presented the results in Figure S6 of the supporting information.

Given that interface forces such as surface tension are approximately negligible at the enormous spatial scale of volcanic systems, slug breakup may be more common in volcanoes than in the laboratory (Suckale, Nave, & Hager, 2010; Suckale, Hager, et al., 2010). However, decompression-related gas expansion and high gas fluxes may stabilize slugs at some volcanoes such as Mount Erebus, Antarctica, where inertial forces are less likely to contribute to slug breakup (Qin et al., 2018) than at some of the other well-studied open-vent volcanoes (Figure 10). Motivated by the possibility that gas slugs may form, we test how core-annular flow modulates slug ascent. We show that slug ascent in core-annular flow shares many similarities with slug ascent in an initially quiescent liquid. The dynamic interactions between the two flow fields are limited in this case, because the ascent speed of the gas slugs is much faster than the average ascent speed of the core liquid (see Figure 4 C). The background flow increases the ascent speed of the slug by a few percent (see Figure 5), similar to the effect of Poiseuille flow on slug ascent (Nicklin et al., 1962), but does not fundamentally alter the ascent dynamics.

Despite its minimal impact on the speed and stability of gas slugs, we argue that the potential presence of exchange flow in volcanic conduits is consequential for understanding the observed variability of eruptive patterns at persistently active volcanoes. Our analogue experiments and numerical simulations demonstrate that the presence of exchange flow entails an inherently more dynamic view of the volcanic conduit than unidirectional flow or a stagnant magma column, because exchange flow introduces an additional interface separating the gas-rich, ascending magma in the core from the degassed, descending magma in the annulus. When gas slugs rise through core-annular flow, the slug interface interacts with the exchange-flow interface with potentially significant consequence for the stability of flow throughout the entire conduit. Our laboratory experiments of rapidly injected gas slugs identify one possible consequence: Rapid extension of the slug volume in a short time creates a wave-like perturbation of the exchange-flow

interface that deforms the slug, leading to slug break-up soon after injection (Figure 6 B_1-B_3).

We emphasize that slug breakup in our laboratory experiments is the consequence of inevitable disruption during injection, as demonstrated when reproducing the laboratory experiments numerically for a variety of injection conditions. In our numerical simulations, we can control injection more completely than possible in laboratory experiments and we find that sufficiently slow and careful injection reduces the dynamic interactions between the two interfaces and leads to stable slug ascent. For comparable inverse viscosity N_f and sufficiently slow injection of gas into the exchange flow, slug stability is comparable for the three flow fields studied here: an initially stagnant liquid, Poiseuille flow and exchange flow (see Figure 7). The onset of breakup in Figure 6 is consistent with the gradual breakup identified previously (Suckale, Hager, et al., 2010). While the slug-injection mechanism used in our laboratory experiments does not translate to volcanic systems (e.g. Blackburn et al., 1976; Jaupart & Vergniolle, 1988), our finding that the dynamic interaction between the two interfaces can fundamentally disrupt the entire conduit-flow regime may. In fact, video "Slug-Core-Annular-V-2" in the online supplement shows the interactions of a standing wave on the exchange-flow interface leading to the breakup of slug and even the core flow.

The delicacy of the dynamic interactions between the slug and the exchange-flow interface in a highly idealized laboratory context suggests the possibility of many additional complexities in actual, inevitably more complex, volcanic systems. For example, sudden changes in the slug volume could arise in response to eruptive processes in the shallow plumbing system such as plug failure (Suckale et al., 2018) or effusive magma removal. Apart from the slug interface, disruptions could also originate at the exchange-flow interface where most of the shear is concentrated, facilitating crystal and bubble nucleation (Tripoli et al., 2019) and coalescence.

The interactions between slug ascent and exchange flow are not limited to exchange flow interrupting slug ascent (see Section 4.3). The ascending gas slug displaces the core liquid around it and, thereby, imposes a localized reversal in the core flow and an increase in the downwards-oriented annulus flow (see Figure 8). While exchange flow can recover from the transient disruption introduced by a single slug, it becomes increasingly prone to collapse or rearrangement the longer sequential slug ascent persists. Our videos of ex-

periment 4e, available in the online supplementary material, record the occurrence of this instability. After a "train" of short slugs (showed in "Slug-Core-Annular-V-1") ascends in exchange flow, a standing wave forms on the exchange flow interface, which interacts with the ascending slug, and leads to the breakup of slug and even the core flow later on (showed in "Slug-Core-Annular-V-2"). One way of re-establishing mass balance would be an effusive eruption that expunges the accumulated surplus mass. It is interesting to note in this context that Stromboli volcano appears to exhibit effusive lava flows after a particularly intense sequence of normal Strombolian eruptions (Ripepe et al., 2017), suggesting a connection between the intensity of one eruptive regime and the occurrence of another. If these normal Strombolian eruptions were to represent large gas slugs, then an intense sequence of Strombolian eruptions could be thought of as multiple, closely-spaced gas slugs and the effusive eruption could represent the expulsion of built-up magma at depth.

We emphasize that this particular interdependence between intense normal Strombolian eruptions and effusive activity is far from ubiquitous and many effusive eruptions are not related to an intense sequence of Strombolian eruptions at all. We mention this example here to highlight the possibility that different eruptive regimes are interdependent and coupled through the internal flow dynamics in the volcanic conduit. This interdependence is probably not limited to effusive and Strombolian eruptions, but would encompass passive degassing, as supported by a recent analysis of long-term eruptive trends at Stromboli, Batu Tara, and Tinakula volcanoes (Laiolo et al., 2018). More important than the specific eruptive regime is the insight that the different flow regimes that may exist in the conduits of persistently active volcanoes, such as slug ascent and core-annular flow, are interdependent with ample opportunity for mutual disruption.

6 Conclusion

We combine analogue experiments and numerical simulations to advance our process-based understanding of the dynamic interplay between slug ascent and exchange flow in the conduits of persistently active volcanoes. We argue that an integrated model framework considering slug ascent and exchange flow jointly, may provide a more comprehensive understanding of persistently active volcanoes than either model in isolation. More specifically, we argue that the interactions between slug ascent and exchange flow iden-

tified here could advance our understanding of the variability of eruptive behavior and the interdependence between different eruptive regimes.

Author Contributions

ZQ performed the numerical simulations and compared the numerical and experimental results. FMB performed the laboratory experiments. ACR conceptualized the laboratory experiments, supported their analysis, and provided volcanological context. JS contributed to the problem formulation, conceptualized the simulations with ZQ and contributed to the analysis of the simulations. All authors contributed to the text.

Acknowledgments

This study was supported by NSF grant 1744758 awarded to JS. FMB would like to thank Matthew Hort for his support, also Jeremy Phillips and Heidy Mader for providing useful feedback on an earlier version of the experimental component presented in this manuscript. The manuscript also benefited from comments from two anonymous reviewers. This manuscript do not entail any original or processed data. All results come from our simulation and experiments. The codes are developed by us for the specific purposes of this paper, which are preserved at http://doi.org/10.5281/zenodo.5030904 ((Qin et al., 2021)).

References

Albert, H., Costa, F., & Martí, J. (2016). Years to weeks of seismic unrest and magmatic intrusions precede monogenetic eruptions. *Geology*, *44*(3), 211–214.

Allard, P. (2010). A CO_2-rich gas trigger of explosive paroxysms at Stromboli basaltic volcano, Italy. *Journal of Volcanology and Geothermal Research*, *189*(3-4), 363–374.

Allard, P., Carbonnelle, J., Métrich, N., Loyer, H., & Zettwoog, P. (1994). Sulphur output and magma degassing budget of Stromboli volcano . *Nature*, *47*, 326-330.

Barmin, A., Melnik, O., & Sparks, R. (2002). Periodic behavior in lava dome eruptions. *Earth and Planetary Science Letters*, *199*(1-2), 173–184.

Beckett, F. M., Mader, H. M., Phillips, J. C., Rust, A. C., & Witham, F. (2011). An experimental study of low Reynolds number exchange flow of two Newtonian fluids in a vertical pipe. *Journal of Fluid Mechanics*, *682*, 652 - 670.

Blackburn, E., Wilson, L., & Sparks, R. J. (1976). Mechanisms and dynamics of strombolian activity. *Journal of the Geological Society*, *132*(4), 429–440.

Bretherton, F. P. (1961). The motion of long bubbles in tubes. *Journal of Fluid Mechanics*, *10*(2), 166–188.

Brown, D. (Accessed 2011). *http://www.cabrillo.edu/ dbrown/tracker/.* Open Source Physics.

Brown, R. (1965). The mechanics of large gas bubbles in tubes: I. Bubble velocities in stagnant liquids. *The Canadian Journal of Chemical Engineering*, *43*(5), 217–223.

Burton, M., Allard, P., Mur, F., & La Spina, A. (2007). Magmatic gas composition reveals the source depth of slug driven Strombolian explosive activity . *Science*, *317*, 227-230.

Capponi, A., James, M. R., & Lane, S. J. (2016). Gas slug ascent in a stratified magma: Implications of flow organisation and instability for strombolian eruption dynamics. *Earth and Planetary Science Letters*, *435*, 159–170.

Collier, L., & Neuberg, J. (2006). Incorporating seismic observations into 2D conduit flow modeling. *Journal of Volcanology and Geothermal Research*, *152*(3-4), 331–346.

Costa, A., Melnik, O., & Sparks, R. S. J. (2007). Controls of conduit geometry and wallrock elasticity on lava dome eruptions. *Earth and Planetary Science Letters*, *260*(1-2), 137–151.

Costa, A., Melnik, O., Sparks, R. S. J., & Voight, B. (2007). Control of magma flow in dykes on cyclic lava dome extrusion. *Geophysical Research Letters*, *34*(2), L02303.

Davies, R. M., & Taylor, G. I. (1950). The mechanics of large bubbles rising through extended liquids and through liquids in tubes. *Proceedings of the Royal Society of London. Series A. Mathematical and Physical Sciences*, *200*(1062), 375–390.

Del Bello, E., Lane, S. J., James, M. R., Llewellin, E. W., Taddeucci, J., Scarlato, P., & Capponi, A. (2015). Viscous plugging can enhance and modulate explosivity of Strombolian eruptions. *Earth and planetary science letters*, *423*, 210–218.

Del Bello, E., Llewellin, E. W., Taddeucci, J., Scarlato, P., & Lane, S. J. (2012). An

analytical model for gas overpressure in slug-driven explosions: Insights into Strombolian volcanic eruptions. *Journal of Geophysical Research: Solid Earth*, *117*(B2).

Dixon, J. E., Stolper, E. M., & Holloway, J. R. (1995). An experimental study of water and carbon dioxide solubilities in mid-ocean ridge basaltic liquids. part i: calibration and solubility models. *J. Petrol*, *36*(6), 1607–1631.

Dumitrescu, D. T. (1943). Strömung an einer Luftblase im senkrechten Rohr. *ZAMM-Journal of Applied Mathematics and Mechanics/Zeitschrift für Angewandte Mathematik und Mechanik*, *23*(3), 139–149.

Firth, C. W., Handley, H. K., Cronin, S. J., & Turner, S. P. (2014). The eruptive history and chemical stratigraphy of a post-caldera, steady-state volcano: Yasur, Vanuatu. *Bulletin of Volcanology*, *76*(7), 1–23.

Fowler, A., & Robinson, M. (2018). Counter-current convection in a volcanic conduit. *Journal of Volcanology and Geothermal Research*, *356*, 141–162.

Francis, P., Oppenheimer, C., & Stevenson, D. (1993). Endogenous growth of persistently active volcanoes. *Nature*, *366*, 554 - 557.

Goldsmith, H., & Mason, S. (1962). The movement of single large bubbles in closed vertical tubes. *Journal of Fluid Mechanics*, *14*(1), 42–58.

Grace, J. R., & Clift, R. (1979). Dependence of slug rise velocity on tube Reynolds number in vertical gas-liquid flow. *Chemical Engineering Science*, *34*, 1348-1350.

Harlow, F. H., & Welch, J. E. (1965). Numerical calculation of time-dependent viscous incompressible flow of fluid with free surface. *Physics of Fluids*, *8*(12), 2182–2189.

Harris, A. J. L., & Ripepe, M. (2007). Temperature and dynamics of degassing at Stromboli. *Journal of Geophysical Research.*, *112*, B3.

Hickox, C. E. (1971). Instability due to viscosity and density stratification in axisymmetric pipe flow. *The physics of Fluids*, *14*(2), 251–262.

Huppert, H. E., & Hallworth, M. A. (2007). Bi-directional flows in constrained systems. *Journal of Fluid Mechanics*, *578*, 95-112.

James, M. R., Lane, S. J., Chouet, B., & Gilbert, J. S. (2004). Pressure changes associated with the ascent and bursting of gas slugs in liquid-filled vertical and inclined conduits. *Journal of Volcanology and Geothermal Research*, *129*,

61-82.

James, M. R., Lane, S. J., & Chouet, B. A. (2006). Gas slug ascent through changes in conduit diameter: Laboratory insights into a volcano-seismic source process in low-viscosity magmas. *Journal of Geophysical Research*, *111*, B05201.

James, M. R., Lane, S. J., & Corder, S. B. (2008). Modelling the rapid and near-surface expansion of gas slugs in low-viscosity magmas. *Geological Society London Special Publications*, *307*, 147-167.

James, M. R., Lane, S. J., Wilson, L., & Corder, S. B. (2009). Degassing at low magma-viscosity volcanoes: Quantifying the transition between passive bubble-burst and strombolian eruption. *Journal of Volcanology and Geothermal Research*, *180*(2-4), 81–88.

Jaupart, C., & Vergniolle, S. (1988). Laboratory models of Hawaiian and Strombolian eruptions. *Nature*, *331*, 58-60.

Jaupart, C., & Vergniolle, S. (1989). The generation and collapse of a foam layer at the roof of a basaltic magma chamber. *Journal of Fluid Mechanics*, *203*, 347–380.

Javoy, M., & Pineau, F. (1991). The volatiles record of a popping rock from the Mid-Atlantic Ridge at 14 N: chemical and isotopic composition of gas trapped in the vesicles. *Earth and Planetary Science Letters*, *107*(3-4), 598–611.

Kang, M., Fedkiw, R. P., & Liu, X. D. (2000). A boundary condition capturing method for multiphase incompressible flow. *Journal of Scientific Computing*, *15*(3), 323–360.

Kazahaya, K., Shinohara, H., & Saito, G. (1994). Excessive degassing of Izu-Oshima volcano: magma convection in a conduit. *Bulletin of Volcanology*, *56*, 207-216.

Kim, J., & Moin, P. (1985). Application of a fractional-step method to incompressible Navier-Stokes equations. *Journal of Computational Physics*, *59*(2), 308–323.

Laiolo, M., Massimetti, F., Cigolini, C., Ripepe, M., & Coppola, D. (2018). Long-term eruptive trends from space-based thermal and SO_2 emissions: a comparative analysis of Stromboli, Batu Tara and Tinakula volcanoes. *Bulletin of Volcanology*, *80*(9).

Llewellin, E., Del Bello, E., Taddeucci, J., Scarlato, P., & Lane, S. (2012). The thickness of the falling film of liquid around a taylor bubble. *Proceedings of the*

Royal Society A: Mathematical, Physical and Engineering Sciences, *468*(2140), 1041–1064.

Llewellin, E. W., Mader, H. M., & Wilson, S. D. R. (2002). The rheology of a bubbly liquid. *Proceedings of the Royal Society of London*, *485*, 987-1016.

Maeda, I. (2000). Nonlinear visco-elastic volcanic model and its application to the recent eruption of Mt. Unzen. *Journal of Volcanology and Geothermal Research*, *95*(1-4), 35–47.

Massol, H., Jaupart, C., & Pepper, D. W. (2001). Ascent and decompression of viscous vesicular magma in a volcanic conduit. *Journal of Geophysical Research: Solid Earth*, *106*(B8), 16223–16240.

Melnik, O., & Sparks, R. (2005). Controls on conduit magma flow dynamics during lava dome building eruptions. *Journal of Geophysical Research: Solid Earth*, *110*(B2).

Métrich, N., & Wallace, P. J. (2008). Volatile abundances in basaltic magmas and their degassing paths tracked by melt inclusions. *Reviews in mineralogy and geochemistry*, *69*(1), 363–402.

Nicklin, D. J., Wilkes, M. A., & Davidson, J. F. (1962). Two phase flow in vertical tubes. *Transactions of the Institution of Chemical Engineers*, *40*, 61-68.

Olsson, E., & Kreiss, G. (2005). A conservative level set method for two phase flow. *Journal of Computational Physics*, *210*(1), 225–246.

Oppenheimer, C., Moretti, R., Kyle, P. R., Eschenbacher, A., Lowenstern, J. B., Hervig, R. L., & Dunbar, N. W. (2011). Mantle to surface degassing of alkalic magmas at Erebus volcano, Antarctica. *Earth and Planetary Science Letters*, *306*(3), 261 - 271.

Oppenheimer, J., Capponi, A., Cashman, K., Lane, S., Rust, A., & James, M. (2020). Analogue experiments on the rise of large bubbles through a solids-rich suspension: a weak plug model for Strombolian eruptions. *Earth and Planetary Science Letters*, *531*, 115931.

Palma, J. L., Calder, E. S., Basualto, D., Blake, S., & Rothery, D. A. (2008). Correlations between SO_2 flux, seismicity, and outgassing activity at the open vent of Villarrica volcano, Chile. *Journal of Geophysical Research*, *113*, B10201.

Parfitt, E., & Wilson, L. (1995). Explosive volcanic eruptionsix. the transition between hawaiian-style lava fountaining and strombolian explosive activity. *Geo-*

physical Journal International, *121*(1), 226–232.

Parfitt, E. A. (2004). A discussion of the mechanisms of explosive basaltic eruptions. *Journal of Volcanology and Geothermal Research*, *134*(1-2), 77–107.

Passarelli, L., & Brodsky, E. E. (2012). The correlation between run-up and repose times of volcanic eruptions. *Geophysical Journal International*, *188*(3), 1025–1045.

Pering, T., McGonigle, A., James, M., Capponi, A., Lane, S., Tamburello, G., & Aiuppa, A. (2017). The dynamics of slug trains in volcanic conduits: Evidence for expansion driven slug coalescence. *Journal of Volcanology and Geothermal Research*, *348*, 26–35.

Picchi, D., Suckale, J., & Battiato, I. (2020). Taylor drop in a closed vertical pipe. *Journal of Fluid Mechanics*, *902*(A19).

Pyle, D. M. (1992). The volume and residence time of magma beneath active volcanoes determined by decay-series disequilibria methods. *Earth and Planetary Science Letters*, *112*(1-4), 61–73.

Qin, Z., Beckett, F. M., Rust, A. C., & Suckale, J. (2021). The code used for qin et al. (2021), interactions between gas slug ascent and exchange flow in the conduit of persistently active volcanoes. *http://doi.org/10.5281/zenodo.5030904*.

Qin, Z., Delaney, K., Riaz, A., & Balaras, E. (2015). Topology preserving advection of implicit interfaces on Cartesian grids. *Journal of Computational Physics*, *290*, 219–238.

Qin, Z., Esmaeilzadeh, S., Riaz, A., & Tchelepi, H. A. (2020). Two-phase multiscale numerical framework for modeling thin films on curved solid surfaces in porous media. *Journal of Computational Physics*, *413*, 109464.

Qin, Z., Soldati, A., Velazquez Santana, L. C., Rust, A. C., Suckale, J., & Cashman, K. V. (2018). Slug Stability in Flaring Geometries and Ramifications for Lava Lake Degassing. *Journal of Geophysical Research: Solid Earth*, *123*(12), 10,431–10,448.

Qin, Z., & Suckale, J. (2017). Direct numerical simulations of gas-solid-liquid interactions in dilute fluids. *International Journal of Multiphase Flow*, *96*, 34–47.

Reinelt, D. (1987). The rate at which a long bubble rises in a vertical tube. *Journal of Fluid Mechanics*, *175*, 557–565.

Ripepe, M., Harris, A. J. L., & Carneil, R. (2002). Thermal, seismic and infra-

sonic evidences of variable degassing rates at Stromboli volcano . *Journal of Volcanology and Geothermal Research*, *118*, 285 - 297.

Ripepe, M., Pistolesi, M., Coppola, D., Delle Donne, D., Genco, R., Lacanna, G., ... Valade, S. (2017). Forecasting effusive dynamics and decompression rates by magmastatic model at open-vent volcanoes. *Scientific Reports*, *7*(1), 1–9.

Seyfried, R., & Freundt, A. (2000). Experiments on conduit flow and eruption behavior of basaltic volcanic eruptions. *Journal of Geophysical Research*, *105*, 23727-23740.

Shinohara, H. (2008). Excess degassing from volcanoes and its role on eruptive and intrusive activity. *Reviews of Geophysics*, *46*(4).

Stevenson, D. S., & Blake, S. (1998, Nov 01). Modelling the dynamics and thermodynamics of volcanic degassing. *Bulletin of Volcanology*, *60*(4), 307–317.

Stoiber, R., & Williams, S. (1986). Sulfur and halogen gases at Masaya caldera complex, Nicaragua: total flux and variations with time. *Journal of Geophysical Research*, *91*, 12,215-12,231.

Stovall, W., Houghton, B. F., Harris, A. J., & Swanson, D. A. (2009). Features of lava lake filling and draining and their implications for eruption dynamics. *Bulletin of volcanology*, *71*(7), 767–780.

Suckale, J., Hager, B. H., Elkins-Tanton, L., & Nave, J.-C. (2010). It takes three to tango: 2. Bubble dynamics in basaltic volcanoes and ramifications for modeling normal Strombolian activity. *Journal of Geophysical Research*, *115*(B7), B07410.

Suckale, J., Keller, T., Cashman, K. V., & Persson, P.-O. (2016). Flow-to-fracture transition in a volcanic mush plug may govern normal eruptions at Stromboli. *Geophysical research letters*, *43*(23), 12–071.

Suckale, J., Nave, J.-C., & Hager, B. H. (2010). It takes three to tango: 1. Simulating buoyancy-driven flow in the presence of large viscosity contrasts. *Journal of Geophysical Research*, *115*(B7), B07409.

Suckale, J., Qin, Z., Picchi, D., Keller, T., & Battiato, I. (2018). Bistability of buoyancy-driven exchange flows in vertical tubes. *Journal of Fluid Mechanics*, *850*, 525–550.

Sussman, M., Almgren, A. S., Bell, J. B., Colella, P., Howell, L. H., & Welcome, M. L. (1999). An Adaptive Level Set Approach for Incompressible Two-Phase

Flows. *Journal of Computational Physics*, *148*(1), 81–124.

Tripoli, B., Manga, M., Mayeux, J., & Barnard, H. (2019). The effects of deformation on the early crystallization kinetics of basaltic magmas. *Frontiers in Earth Science*, *7*, 250.

Vergniolle, S., & Jaupart, C. (1986). Separated two-phase flow and basaltic eruptions. *Journal of Geophysical Research*, *91*(B12), 12842–12860.

Vergniolle, S., & Mangan, M. (2000). Hawaiian and Strombolian eruptions. In *Encyclopedia of volcanoes* (pp. 447–461).

Viana, F., Pardo, R., Yanez, R., Trallero, J. L., & Joseph, D. D. (2003). Universal correlation for the rise velocity of long gas bubbles in round pipes. *Journal of Fluid Mechanics*, *494*, 379-398.

Vitturi, M. d., Clarke, A., Neri, A., & Voight, B. (2008). Effects of conduit geometry on magma ascent dynamics in dome-forming eruptions. *Earth and Planetary Science Letters*, *272*(3-4), 567–578.

Wallis, G. B. (1969). *One dimensional two-phase flow.* McGraw Hill.

White, E., & Beardmore, R. (1962). The velocity of rise of single cylindrical air bubbles through liquids contained in vertical tubes. *Chemical Engineering Science*, *17*(5), 351–361.

Wilson, L. (1980). Relationships between pressure, volatile content and ejecta velocity in three types of volcanic explosion. *Journal of Volcanology and Geothermal Research*, *8*(2-4), 297–313.

Zukoski, E. (1966). Influence of viscosity, surface tension, and inclination angle on motion of long bubbles in closed tubes. *Journal of Fluid Mechanics*, *25*(4), 821–837.